5

Solvent dependent fabrication of binary nanoparticles and nanostructured thin films by self assembly of functional alkoxysilanes

---

5.1. INTRODUCTION

Assembling the nanoparticles into ordered thin films of uniform thickness with precisely controlled surface properties is a challenging task. Several techniques have been explored to design thin films, compatible for practical applications (Joo et al., 2001; Fu et al., 2005; Yuan et al., 2005; Ibn-Elhaj et al., 2001), which include the electrodeposition of semiconductor and metal nanoparticles (Quinn et al., 2005), the deposition of nanoparticle monolayers via the Langmuir Blodgett technique (Paul et al., 2003), sol-gel method (Tadanaga et al., 2000) and in situ synthesis of nanoparticles using polymeric thin films as templates (Lee et al., 2006; Boontongkong and Cohen, 2002; Pietsch et al., 2015; Wadley et al., 2012). These techniques did not ensure the retention of noble metal nanoparticles with average diameter 5-8 nm. Therefore, in order to withhold nanoscaled particles (below 8 nm), it is required to fabricate uniform and nanostructured thin films.

In this chapter, the possibility of creating suitable thin films using functional alkoxysilanes like 3-aminopropyltrimethoxysilanes (APTMS), epoxycyclohexyl ethyltrimethoxysilane (EETMS)

(Pandey et al., 2003) has been investigated. Silane mediated thin films often turn into sol-gel monoliths due to iterative cycles of hydrolysis and polycondensation (Radin et al., 2001). Here the synthesis of palladium based (Pandey and Singh, 2014) bimetallic nanoparticles (Au@Pd (Pandey and Singh, 2014; Pandey and Singh, 2015; Pandey and Pandey, 2016) and Ag@Pd) using the organofunctionalised alkoxysilanes, (EETMS and APTMS) as reducing and stabilizing agents (Pandey and Singh, 2014; Pandey and Singh, 2015; Pandey and Pandey, 2016) has been discussed. Bimetallic counterparts of noble metals Pd, Au and Ag are studied due to the remarkable catalytic performance (Maenosono et al., 2017; Fu et al., 2013; Fageria et al., 2016; Anandan et al., 2008; Liz-Marzan and Philipse, 1995; Torigoe K, Esumi, 1993; Tsuji et al., 2006). These metals have similar lattice parameters (Pd= 0.39, Ag=0.409 and Au=0.408 nm) which promotes the excellent electronic distribution between them (Fu et al., 2013; Fageria et al., 2016; Anandan et al., 2008; Liz-Marzan, Philipse, 1995; Torigoe K, Esumi, 1993; Tsuji et al., 2006; Srnova et al., 2000) and in turn also facilitates their facile synthesis.

In this chapter, synthesis of bimetallic colloids proceeds through sequential wet chemical reduction pathway. The general process involved, the reduction of Pd^{2+} to Pd^{0} where EETMS acts as reducing agent, and conversion of Au^{3+}/Ag^{+} to Au^{0}/Ag^{0} involves APTMS as stabilizing and formaldehyde as reducing agents (Pandey and Singh, 2015; Pandey and Pandey, 2016). Obtained colloidal dispersions do not experience hardening or sol-gel glass formation and it can be stored as such for months. Indeed this approach relies on regulating the water content in the corresponding nanostructured thin films. Accordingly, we have tried nonaqueous solvent based synthesis of the nanoparticles, with the optimum amount of water (10^{-6} M). The deposition of thin film on ITO glass substrates initiates the surface fastened ligands (residual groups of

functionalized alkoxysilanes, EETMS and APTMS) on core-shell structured hybrid nanoparticles to condense with silanol groups in proximity (Bunker et al., 2000), and undergo gradual sol-gel process (Pandey et al., 2005; Hancock et al., 2017). The micellar behavior of APTMS (Pandey and Singh, 2015; Pandey and Pandey, 2016) stimulates the nanoparticles to stay in ordered nanodomains and fortifies the self assembly of such hybrid stuff (Pietsch et al., 2015). The substrate-surface interactions are fine tuned, which ensure the stability of the film and allows the deposition of well defined structures rather than extended objects like lamellar aggregates etc, which is confirmed by AFM (Pietsch et al., 2015). This technique provides much simple criteria to construct arrays of nanoparticles on solid substrates simply by dip coating of colloidal dispersion of micelles containing nanoparticles. The thickness and porosity of film are studied using atomic force microscopy (AFM) (Pietsch et al., 2015; Bunker et al., 2000). Such thin films can act as effective heterogeneous catalysts for numerous catalytic applications. One of the potential applications of such thin films is the electrochemical sensing of bioanalytes (Majdi et al., 2007; Heli et al., 2009; Ogura et al., 1999). Present approach does involve organofunctionalised alkoxysilanes but direct ordering of hydrocarbon chains to form dense sol-gel glass layer (Bunker et al., 2000) on the substrate is prevented here. Instead of encapsulating functional nanoparticles into a prefabricated matrix of organically modified silicates (sol-gel matrix) (Pandey et al., 2005), construction of a matrix of organosilanes, and synthesis of the nanoparticles is carried out simultaneously. The film processing variables are identified and optimized (Lee et al., 2006), to cast monolayered thin films with enhanced catalytic activity and controlled sol-gel processing (Hancock et al., 2017). Typically, block-copolymer based thin film (Pietsch et al., 2015; Wadley et al., 2012) formation in the order of tens of nm thickness has been

reported till now. In this chapter the fabrication of core structured binary nanoparticles on solid substrate in an ordered pattern thin films with reduced thickness (5-9 nm) has been demonsrated, using organofunctionalised alkoxysilanes (EETMS, APTMS), and also the electrochemical investigations on the thin film modified electrodes have been reported.

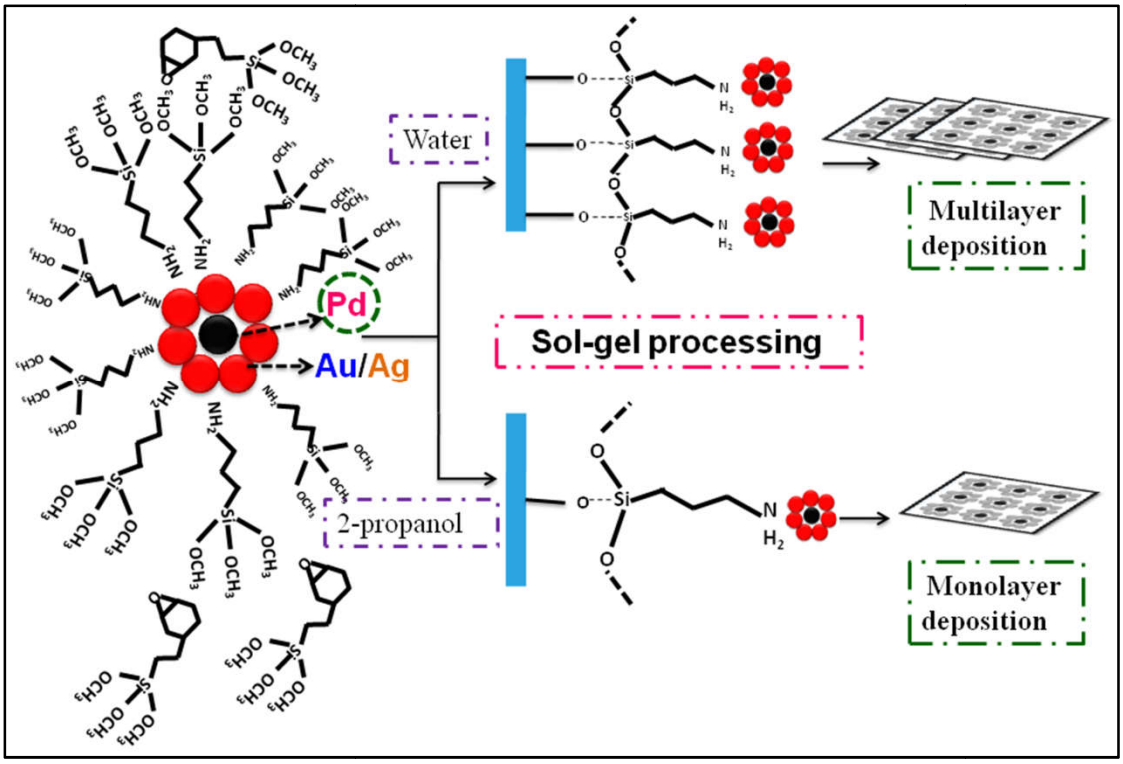

Scheme 5.1. Pictorial representation of effect of sol-gel processing in deposition of a self assembled monolayer.

5.2. EXPERIMENTAL SECTION

5.2.1. Materials

Potassium tetrachloropalladate(II) (K_2PdCl_4), Hydrogen tetrachloroaurate(III) ($HAuCl_4$), silver nitrate ($AgNO_3$), poly(N-vinyl-2-pyrrolidone (PVP), 3-aminopropyltrimethoxysilane (APTMS),

2-(3,4-epoxycyclohexyl) ethyltrimethoxysilane (EETMS) and ITO coated glass were purchased from Sigma aldrich while formaldehyde solution from Merck India. Millipore double distilled water was used for the experiments.

5.2.2. Solvent dependent synthesis of PdNPs, Au@PdNPs and Ag@PdNPs

The stock solutions of each, K_2PdCl_4 (10 mM, 0.0017 g), $AgNO_3$ (10 mM, 0.0016 g), $HAuCl_4$ (10 mM, 0.0039 g), APTMS (1 M, 18 μL) and EETMS (0.5 M, 115 μL) were separately prepared in water, methanol and 2-propanol respectively. 1% solution of PVP was prepared in distilled water. In brief, PdNPs, Au@PdNPs and Ag@PdNPs were synthesised via chemical reduction of inorganic precursors. Initially, Pd^{2+} is rapidly converted to Pd^0 using EETMS as reducing agent in the presence of PVP as stabilizer in water, methanol, and 2-propanol following the same steps as discussed in previous chapters. The yellowish black homogenous dispersion of palladium nanoparticles are obtained in all mediums. Further, the corresponding bimetallic nanoparticles (Au@PdNPs and Ag@PdNPs) are synthesized in corresponding solvents, via sequential or successive reduction of the Au^{3+} and Ag^{+} ions, by following seed-mediated growth phenomenon. Typical synthesis involve, the addition of 40 μL of APTMS capped Au^{3+} (micellar solution) to 60 μL of PdNPs colloidal solution, followed by the addition of formaldehyde to this mixture. The color changes to blackish red, which indicates the formation of bimetallic Au@PdNPs. Similarly, Blackish yellow colloidal solution of Ag@PdNPs was obtained in water, methanol, and propanol.

5.2.3. Thin film deposition and electrochemical measurements

Indium Tin Oxide (ITO) glass (25 mm × 25 mm × 1.1 mm) with resistivity 8-12 Ω/sq was used for depositing the film of nanoparticles. The chemical composition of the ITO coated glass taken

is 74% In, 18% O_2 and 8% Sn by weight. ITO glass was primarily cleaned by soaking it in propanol and acetone for 2-3 hours and sonicated for 5-6 times and finally dried in nitrogen atmosphere. Further cleaned by ultrasonication in a mild acidic solution (0.001 M HCl) for 15 minutes; the process was repeated for about 5-10 times. Thereafter, the substrate was rinsed using Millipore distilled water to remove excess of acid and after rinsing with acetone substrate was dried at 80 ºC for ~10 min. ITO is known for its remarkable optical transparency and conductivity, therefore it is well suited for effective thin film formation. Nanoparticle solutions were dip coated on the glass substrates using 8 wt % solutions of all the colloidal systems (PdNPs, Au@PdNPs, and Ag@PdNPs) in water, methanol and 2-propanol at a dipping speed of 550 mm per minute. ITO was held orthogonally, maximum for 4 s and withdrawn out of the sol. After withdrawing the substrate it was dried in vacuum for ~2-3 hours, followed by washing the films with acetone to remove the unattached portions of the coated solutions. AFM measurements were performed to evaluate the solvent dependent changes in thickness, pore density, and topographical features. Based on the characteristic features, 2-propanol based thin films of different nanoparticle systems are tried as the electrochemical catalysts. Alkoxysilane based thin films are loaded on glassy carbon electrode (GCE) by dip coating of bulk solutions. Electrochemical measurements were performed on CHI830b Electrochemical Analyser using three electrode systems with a working volume of 3 mL, where thin film modified GCE are used as working electrodes, with graphite plate as a counter and Ag/AgCl as reference electrodes.

5.2.4. Characterization of bifunctional nanomaterials

Transmission electron microscopy (TEM; Technai G2, 20 TWIN 50/60 Hz 210-240 V, 943205022121, the FEI Czech Republic with accelerating voltage 200 kV) was used to evaluate

the morphological features of as-synthesized nanocomposites. Colorimetric analysis has been done using UV spectrophotometer (Hitachi U 2900, Hitachi Hi-Tech technologies, Tokyo Japan). Measurements were done in 1 cm quartz cuvette in the wave length range of 200–600 nm. HR-XRD (SMART LAB, RIKAGU Corporation, 900 W, 45kV, 200 mA, target-Cu, detector-DTex Ultra 250, Akishima, Japan) was used to obtain diffractograms of the materials divulged to higher temperatures. AFM studies were brought about by NT-MDT, NTEGRA TRIMA with scanning mode—semi contact/tapping mode, with a monochromatic laser beam of wavelength 650 nm and frequency 150 Hz. Dynamic light scattering (DLS) (Malvern) measurements were carried out to investigate the formation of micellar structure and the possibility of mono and multilayer formation on the deposition of bulk solutions, as a function of solvent selective hydrodynamic radius (R_H).

5.3. RESULTS

5.3.1. Binary nanoparticle synthesis and characterisation

Bimetallic nanoparticles are prepared by wet chemical synthesis via seed-mediated growth phenomenon (Millstone et al., 2008; Jana et al., 2001; Wu et al., 2010) using the presynthesized palladium nanoparticles. The sequential synthesis of core structured binary nanoparticles, Au@PdNPs and Ag@PdNPs (Pandey and Singh, 2014; Pandey and Singh, 2015; Pandey and Pandey 2016; Teng et al., 2003; Sounart et al., 2006) is made possible by the combined action of two alkoxysilanes, EETMS and APTMS, with different functionalities. The chapter focuses on the synthesis of palladium-based binary nanoparticle dispersions, with an aim to fabricate core structured bifunctional nanoparticles on a solid substrate in an ordered pattern thin film (Pietsch et al., 2015).

The reduction of gold and silver ions to form the palladium based bimetallic nanoparticles is observed by visual change in color, from brownish black to dark reddish-black in case of Au@PdNPs while to yellowish-black for Ag@PdNPs. The characteristic color variations were observed within 10-15 minutes. The synthesis of Au@PdNPs and Ag@PdNPs nanoclusters was studied using UV-VIS spectroscopy or SPR technique as a function of the ratio of precursors and the solvent in which synthesis is carried out. The UV-Vis spectra in Figure 5.1 clearly demonstrate the shift in absorption maxima, depending on the concentrations of $HAuCl_4$ and 3-APTMS in Au@PdNPs and 3-APTMS alone in Ag@PdNPs (Xiao et al., 2014; Pozun et al., 2013).

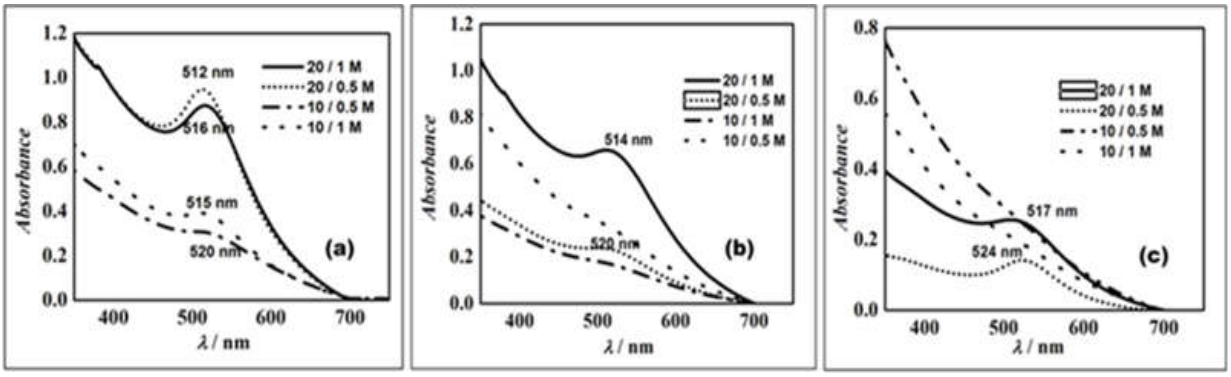

Figure 5.1. UV-Vis absorption spectra of bimetallic Au@PdNPs at different concentrations of precursors ($HAuCl_4$/APTMS), in (a) propanol, (b) methanol and (c) water.

The effect of Au^{3+}/APTMS ratio on the formation of Au@PdNPs, in three different solvents (water, methanol, and propanol) is examined colorimetrically using (Figure 5.1). At higher Au^{3+} content (20 mM) and 1 M APTMS, the absorbance recorded was highest in all the solvents (Figure 5.1a-c). A blue shift in absorbance maxima (smaller mean particle size), is observed in case of 20 mM $HAuCl_4$/1 M APTMS, while at lower Au^{3+} content (10 mM), a red shift in

plasmon resonance is obtained (bigger average diameter). Further, the lowest absorbance maxima, i.e, 512 nm is observed in 2-propanol, attributing to the smallest particle size of Au@PdNPs in 2-propanol. The absence of any strong absorption in the visible region, confirms no sign of Au-Pd alloy formation (Xiao et al., 2014). Similarly, Figure 5.2a-c shows solvent dependent behavior of the molar ratio of precursors in case of Ag@PdNPs was studied (He et al., 2003). In methanol, at higher concentrations of APTMS the characteristic peak of silver nanoparticles (Ag^0) is observed, while in 2-propanol, characteristic peak is recorded at a lower concentration of APTMS. Further, the occurrence of characteristic plasmon bands of Au^0 and Ag^0 around 520 and 410 nm absorption bands, justify the retention of individual character of gold and silver nanoparticles (Xiao et al., 2014) in bimetallic forms.

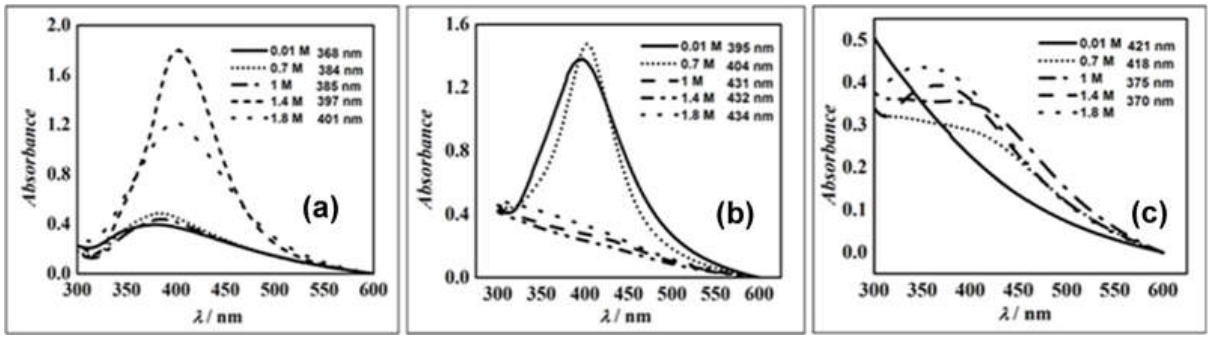

Figure 5.2. UV-Vis absorption spectra of bimetallic Pd-AgNPs at different concentrations of precursor (APTMS), in (d) propanol, (e) methanol and (f) water.

Morphological characters were analysed by transmission electron microscopy (TEM) (Pozun et al., 2013; Hu et al., 2003). TEM images reveal that the cluster like morphology of Palladium nanoparticles (Figure 5.3) completely transformed to spherical seed, which forms the core, encircled by the shell of Ag / Au in bimetallic analogues. Bimetallic nanoparticles are almost spherical in shape (Figure 5.4), with average diameters of 4.1 ± 0.05 nm and 5.2 ± 0.10 nm, for

Au@PdNPs and Ag@PdNPs, as compared to PdNPs, around 13.5 ± 0.97 nm (Figure 5.3a), which is considerably higher than those of bimetallic analogues. The exterior shell consists of Au and Ag in surplus along with Pd in feeble amount. The existence of Au/Ag in excess, significantly matches with the ratio in which the precursors were fixed initially [K_2PdCl_4/$HAuCl_4$ (1:4) and K_2PdCl_4/$AgNO_3$ (1:5)].

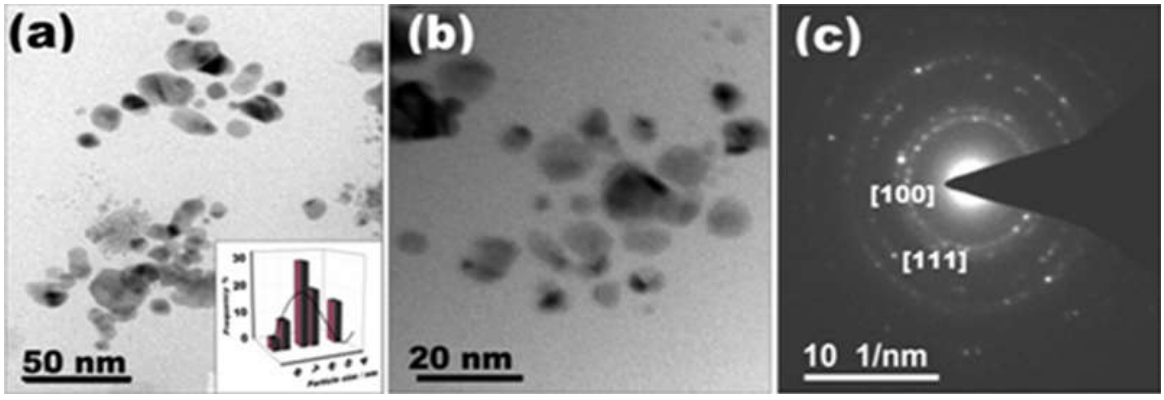

Figure 5.3. TEM images (a)-(b), and corresponding SAED pattern of PdNPs (c). Inset to picture (a) shows the particle size distribution analysis.

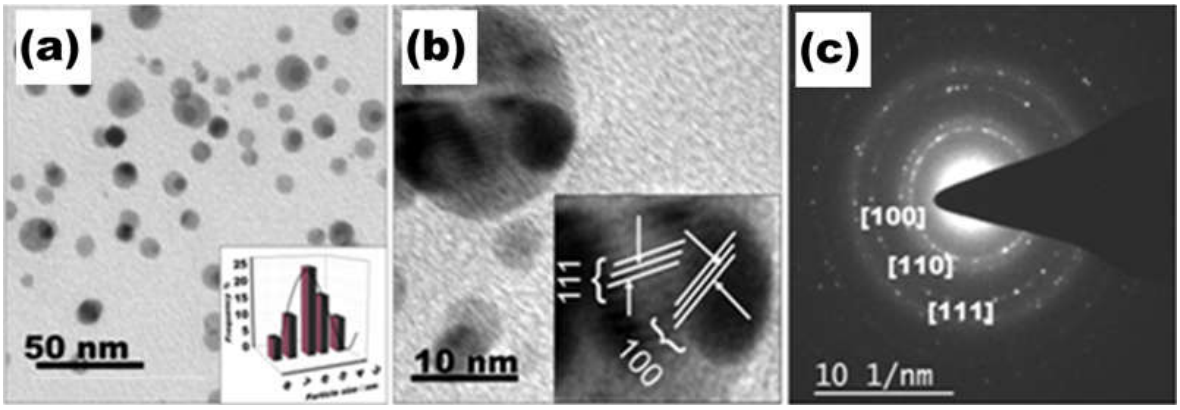

Figure 5.4. TEM images (a)-(b), and corresponding SAED pattern of Au@PdNPs (c). Inset to picture (a) shows the particle size distribution analysis. Inset to images (b) displays the lattice fringes.

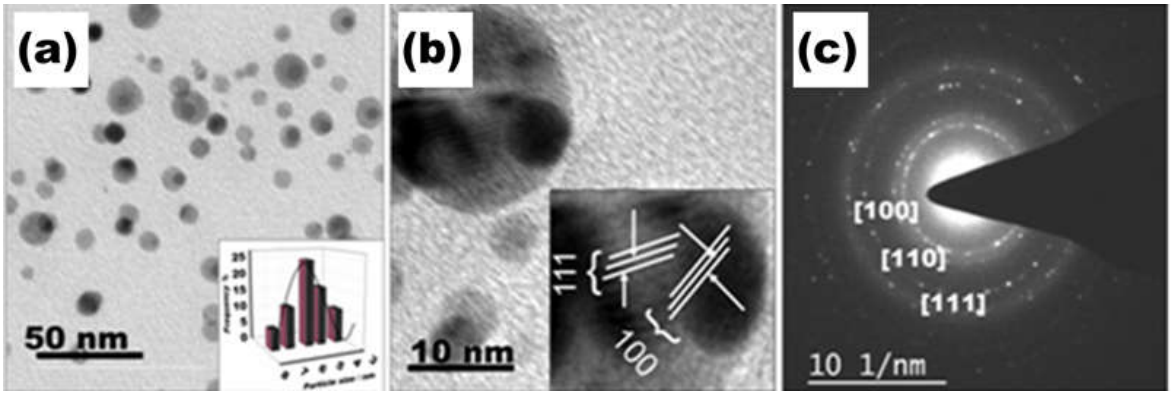

Figure 5.5. TEM images (a)-(b), and corresponding SAED pattern of Ag@PdNPs (c). Inset to picture (a) shows the particle size distribution analysis. Inset to images (b) displays the lattice fringes.

Au@PdNPs typically displayed five characteristic reflections, 28.27^{o} , 38.72^{o} , 40.586^{o} , 66.52^{o} and 73.798^{o} (Kobayashi et al., 2009) with corresponding lattice planes [100], [111], [200], [220] (Figure 5.8). The lattice fringes observed in Au@PdNPs (Pandey and Pandey 2016; Lim et al., 2010) representing the antiparallel planes, (100) and (111) with lattice spacing 0.023 and 0.018 nm, while in Ag@PdNPs the bright parallel lattice fringes are observed (He et al, 2003), which correspond to the plane (111), with a lattice spacing of 0.020 nm. The Selected Area Electron Diffraction (SAED) pattern (Figure 5.3c) of PdNPs correspond to {100} and {111} facets, in contrast Au@PdNPs consists of prominent facets: (100), (110) and (111) (Lim et al, 2010) (Figure 5.4c), while Ag@PdNPs account for (111), (200) and (311) (Figure 5.5c) respectively. EDS maps (Figures 5.6 and 5.7) show the core-shell arrangement of the metal (Au/Ag) nanoparticles in hybrid corresponding nanohybrids (Au@PdNPs and Ag@PdNPs).

XRD technique gives a deeper insight into the crystal structures, their orientation about crystallographic axes, and other lattice properties. Diffractogram of PdNPs, exhibits four major reflections, 40.3^{o}, 46.7^{o}, 68.29^{o} and 82.29^{o} with successive decrease in intensity due to

broadening of peaks (Wojcieszak et al., 2010) and these reflections are indexed with planes, [111], [200], [220] and [311] (Figure 5.8), The d-value of the reflection [111] is the highest, while for [311] it is the lowest, along with the reduction in lattice strain (from 0.020 - 0.0080). Further, the d-spacing values for reported reflections in case of Au@PdNPs were found to increase in comparison to the similar crystalline phases in monometallic PdNPs.

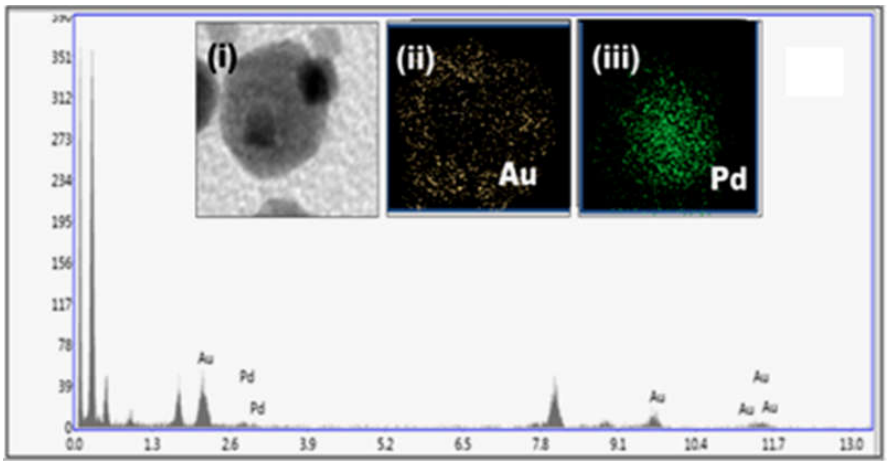

Figure 5.6. EDS profile of Au@PdNPs. Inset shows the TEM image (i) elemental maps of Au and (ii) Pd in Au@PdNPs.

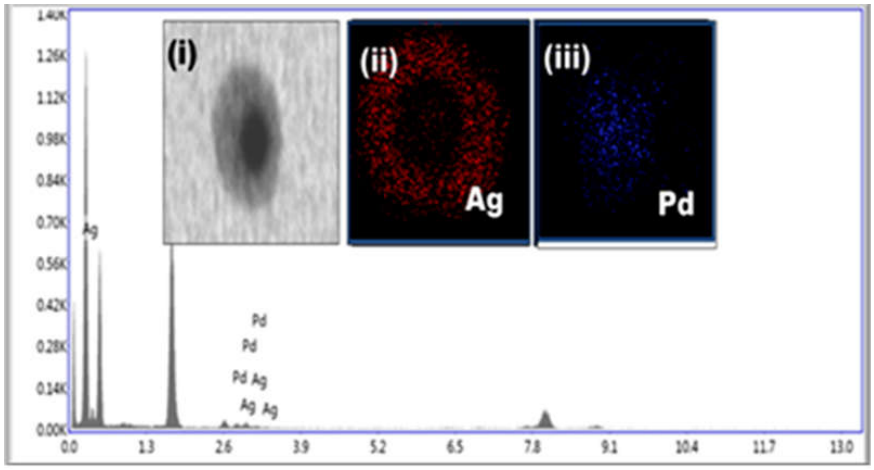

Figure 5.7. EDS profile of Ag@PdNPs. Inset shows the TEM image (i) elemental maps of Ag and (ii) Pd in Ag@PdNPs.

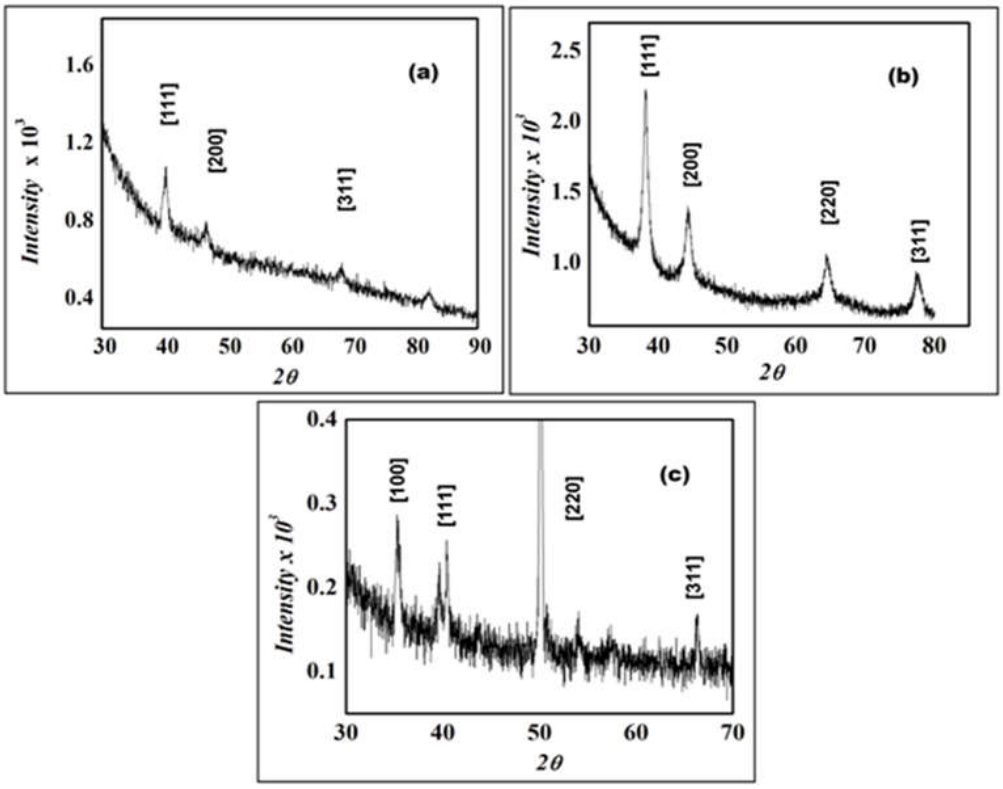

Figure 5.8. X-ray diffraction patterns of (a) PdNPs, (b) Au@PdNPs and (c) Ag@PdNPs.

Similarly, Ag@PdNPs nanoparticles displayed following reflections (Pd/Ag feeded in the molar ratio 1:1), 38^{o} (major), 43^{o} (weak), (Na et al., 2010) with lattice planes [111], [200] respectively. The peaks shown in diffractogram (Figure 5.8) possess declined intensities, which demonstrate the decreased relative crystallinity of Ag@PdNPs, but the average crystallite sizes are increased relative to PdNPs, which is in synchronisation with the TEM analysis.

Surface properties of nanoparticles were studied using X-ray photoelectron spectroscopy (XPS) (Chen et al., 2011; Chen et al., 2011; Tsuji et al., 2016). As visualized from the XPS spectrum (Figure 5.9) the metal at the core shows well-defined peaks at respective binding energies while

the element contributing the shell display considerable shift in binding energies, with peaks reduced in intensity. Eloquent existence of Pd 3d, Au 4f and Ag 3d peaks in Pd-Au and Pd-AgNPs supports the evolution of bimetallic nanoparticles. XPS spectra of Palladium nanoparticles consists of a clearly resolved doublet (Chen et al., 2011) ($3d_{5/2}$ & $3d_{3/2}$) with peaks assigned at ~ 335 and 340 eV in monometallic (PdNPs) and bimetallic (Au@Pd & Ag@PdNPs) analogues. A fall-off in relative peak intensities was recorded from monometallic to bimetallic Palladium. The intensity ratios for nanoparticles are: PdNPs $I(3d_{5/2})$: $I(3d_{3/2})$ = 1.92 (in monometallic); $I(3d_{5/2})$: I $(3d_{3/2})$ = 2 (in Au@PdNPs); $I(3d_{5/2})$: $I(3d_{3/2})$ = 2.8 (in Ag@PdNPs), suggesting that the intensity ratio in case of Ag@PdNPs absolutely matches with the standard ratio of $3d_{5/2}$: $3d_{3/2}$ = 3 (Figure 5.9). XPS Au 4f spectra of Au@PdNPs shows a doublet with peaks $4f_{7/2}$ and $4f_{5/2}$ at binding energies around ~82.4 and 84.6 eV, which are 1.6 and 2.9 eV lower than the bulk values. While, XPS Ag 3d spectra of Ag@PdNPs presents doublet with peaks $3d_{5/2}$ and $3d_{3/2}$ at ~368 and 372.4 eV. The binding energy of Ag $3d_{3/2}$ is shifted to lower end, which is around 1.6 eV below standard bulk values for Ag. $4f_{7/2}$ Au and $3d_{5/2}$ Ag peaks show broadening which is probably due to the changes in chemical envoirment of one metal by another and also instrumental constraints.

5.3.2. Fabrication of solvent dependent thin films

Balanced interactions between hydrophilic and hydrophobic (Pandey et al., 2005; Hupka et al., 2010; Tareste et al., 2007; Tadanaga et al., 2000) alkoxysilanes (APTMS and EETMS) in different solvents provide an effective platform for laying down a proper framework of the fluid thin film.

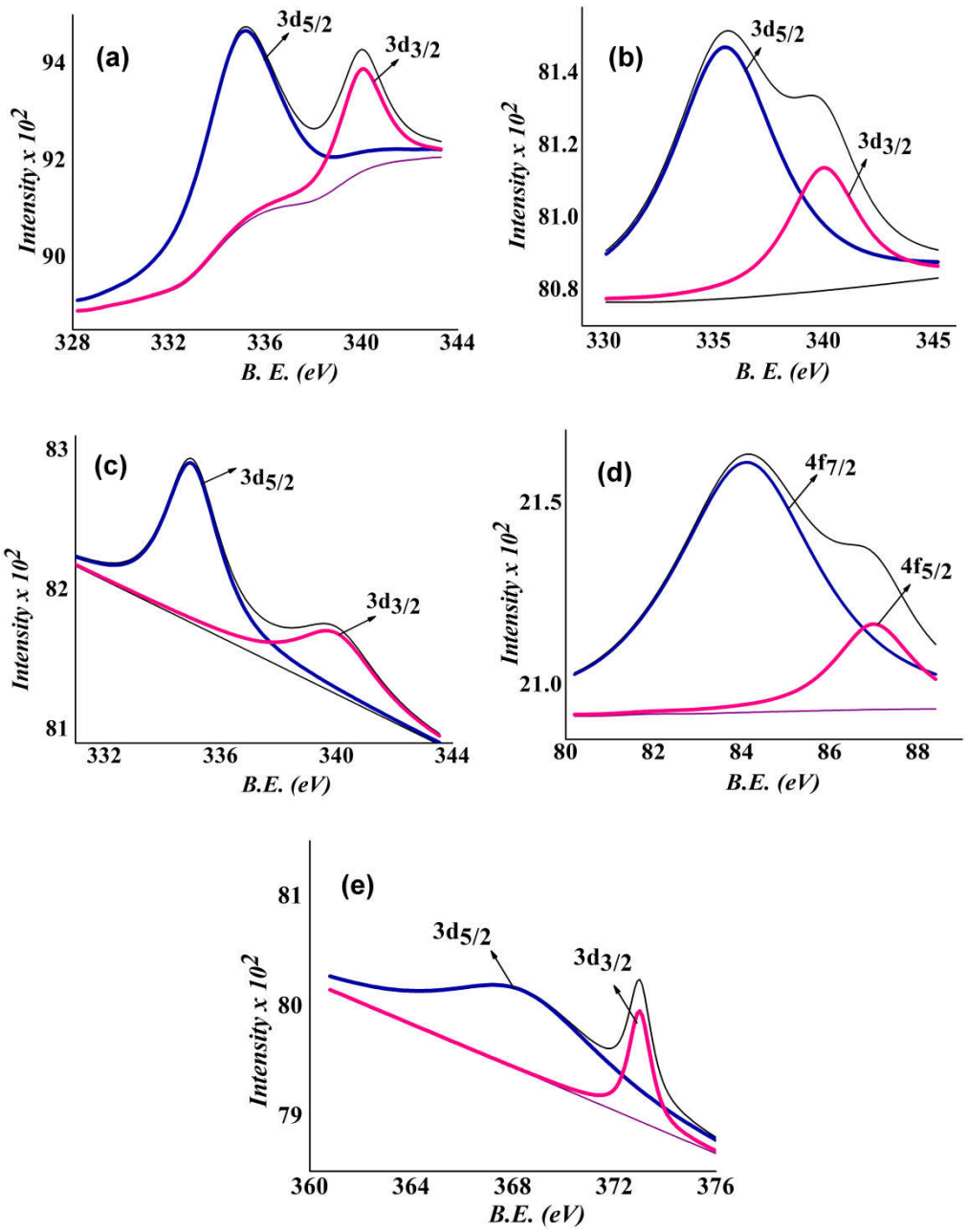

Figure 5.9. XPS spectra of Pd 3d in (a) PdNPs, (b) Au@PdNPs and (c) Ag@PdNPs; (d) Au 4f in Au@PdNPs and (e) Ag 3d in Ag@PdNPs respectively.

The micellar activity of APTMS (Pandey and Singh, 2014; Pandey and Singh, 2015; Pandey and Pandey, 2016) and film forming ability of EETMS via sol gel processing support the assembling of organized uniform thin films with precise control over nanogeometry. Here the bifunctional nanomaterials (Au@PdNPs and Ag@PdNPs) are self-assembled into a patterned array to form monotonous thin film, mainly in alcoholic medium. AFM micrographs (Figure 5.10-5.12) show the variation in film thickness depending on the solvent. The propanol based nanoparticle systems, probably generate a thin film with an average thickness of 6-8 nm, which is relatively thinner than water (13-14 nm) and methanol (9-11 nm) analogues. The growth behavior of layers of thin film comprising mono and bifunctional nanoparticles is monitored by parameters like thickness and root mean square (RMS) roughness (R_{sq}). The variation in root mean square roughness (R_{sq}) also depends on the solvent system. The observed increase in surface roughness (Table 5.1) for aqueous system is due to the non uniform coating combined with probable multilayer deposition of the bulk solution. While in alcoholic systems the values of R_{sq} were relatively lower. In addition, the average pore diameters of the thin films are also a direct function of solvent systems, which are in the order, 8.7, 5.8 and 3.6 (Figure 5.10-5.12) nm with mean pore densities of 22, 29, 35% for water (Figure 5.10d-f), methanol (Figure 5.11d-f) and propanol (Figure 5.12d-f) based systems. Further, noticeable shift in surface topography from upward projected structures to dense populated or congested nanostructured lattice is observed (Figure 5.10-5.12), which shows a clear dependency of morphology and orientation of objects in the deposited thin films, on the solvent selection. Water-based thin film show primarily few featureless regions, inconsistent lamellar structures and alternate bright and dull regions, in propanol (Figure 5.12).

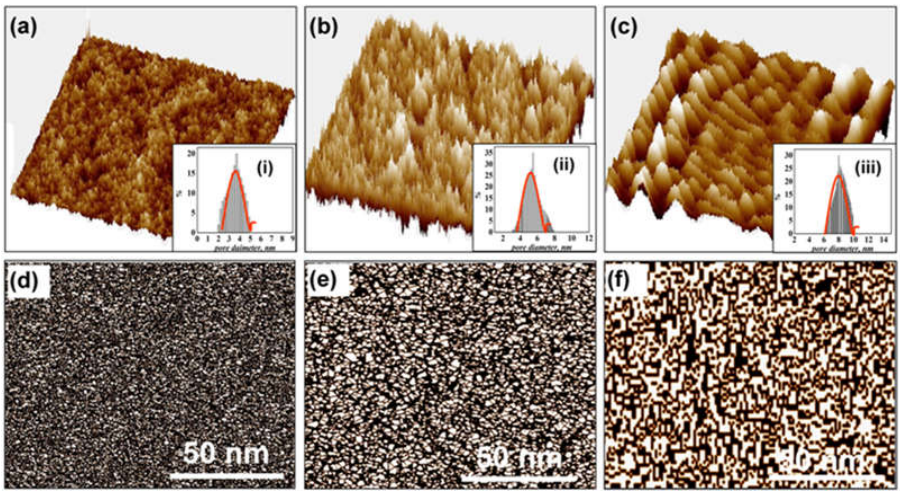

Figure 5.10. AFM topographies of (a) Au@PdNPs, (b) Ag@PdNPs and (c) PdNPs, in water (d)-(f) The grain size distribution analysis of Au@PdNPs, Ag@PdNPs and PdNPs. Inset to the figures (a)-(c) shows the pore size distribution.

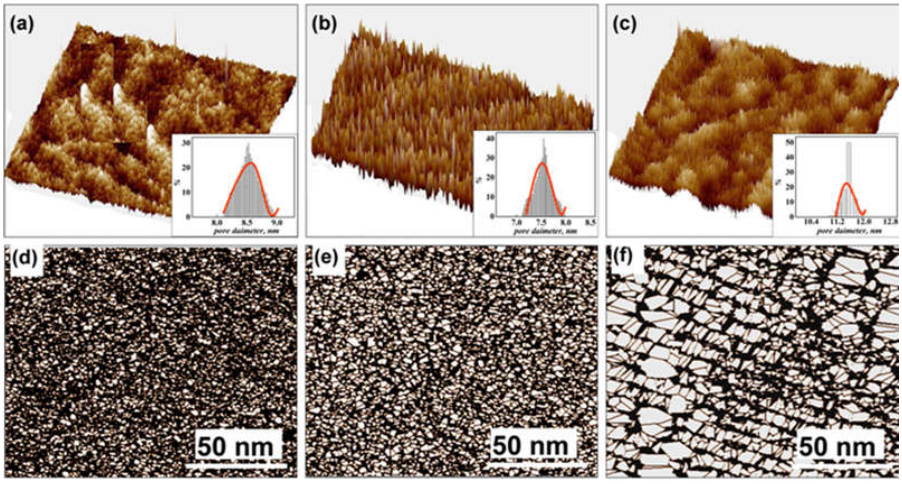

Figure 5.11. AFM topographies of (a) Au@PdNPs, (b) Ag@PdNPs and (c) PdNPs, in methanol. (d)-(f) The grain size distribution analysis of Au@PdNPs, Ag@PdNPs and PdNPs. Inset to the figures (a)-(c) shows the pore size distribution.

Dense arrangement of objects and significantly high pore density is observed in methanol and even higher in propanol based bifunctional nanoparticles synthesized using EETMS and APTMS (Au@PdNP, Ag@PdNPs). Analysis of cross-sectional outlines reveals the thickness, grain sizes,

pore densities, regularity of the film and corresponding roughness of the coated substrates in different cases.

DLS results suggest that the configuration of objects formed considerably depends on the solvents used (Pietsch et al., 2015). It confirms the formation of solvent specific structures with unique hydrodynamic diameter (Park et al., 2008), and corresponding polydispersity indices of all the systems (Figure 5.13). The difference in z-average values of monometallic nanoparticles (PdNPs), fabricated using two different reactions schemes (a) K_2PdCl_4/ PVP/EETMS, (b) K_2PdCl_4/APTMS/HCHO), suggests the possibility of different kind of interactions with metallic species.

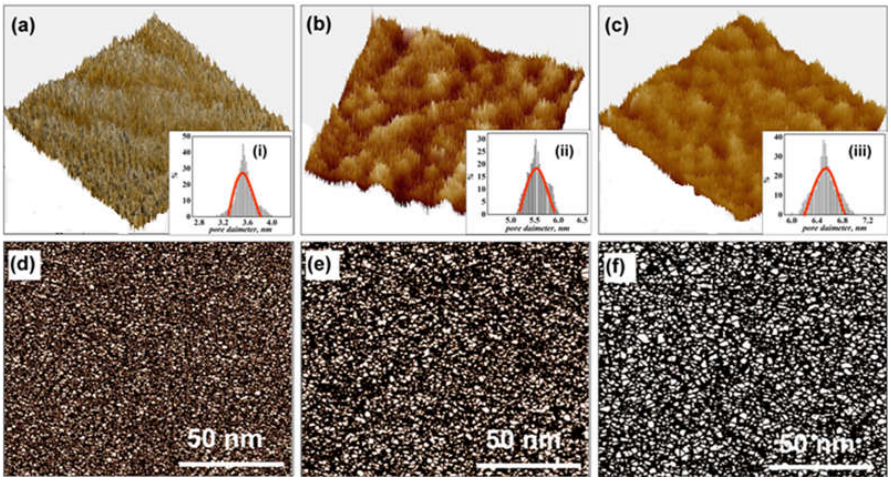

Figure 5.12. AFM topographies of (a) Au@PdNPs, (b) Ag@PdNPs and (c) PdNPs, in 2-propanol. (d)-(f) The grain size distribution analysis of Au@PdNPs, Ag@PdNPs and PdNPs. Inset to the figures (a)-(c) shows the pore size distribution.

5.3.3. Electrochemical catalysis using thin film modified electrodes

The thin films of as prepared nanoparticles are evaluated as electrocatalysts for sensing applications. The ordered arrangement of nanocatalysts in the form of nanostructured thin film, provides effective surface area and enhanced exposure to the analyte during electrochemical

reaction. Cyclic voltammograms of 0.1 M L-Trp were recorded at different pH, using thin film modified, glassy carbon electrodes (GCE), at a potential range of 0.4-1.2 V. L-Trp undergoes an irreversible oxidation i.e, a anodic peak at potential window ranging between 0.6-0.8 V is observed in forward scan (Figure 5.14) while reverse scanning does not involve any corresponding cathodic peak.

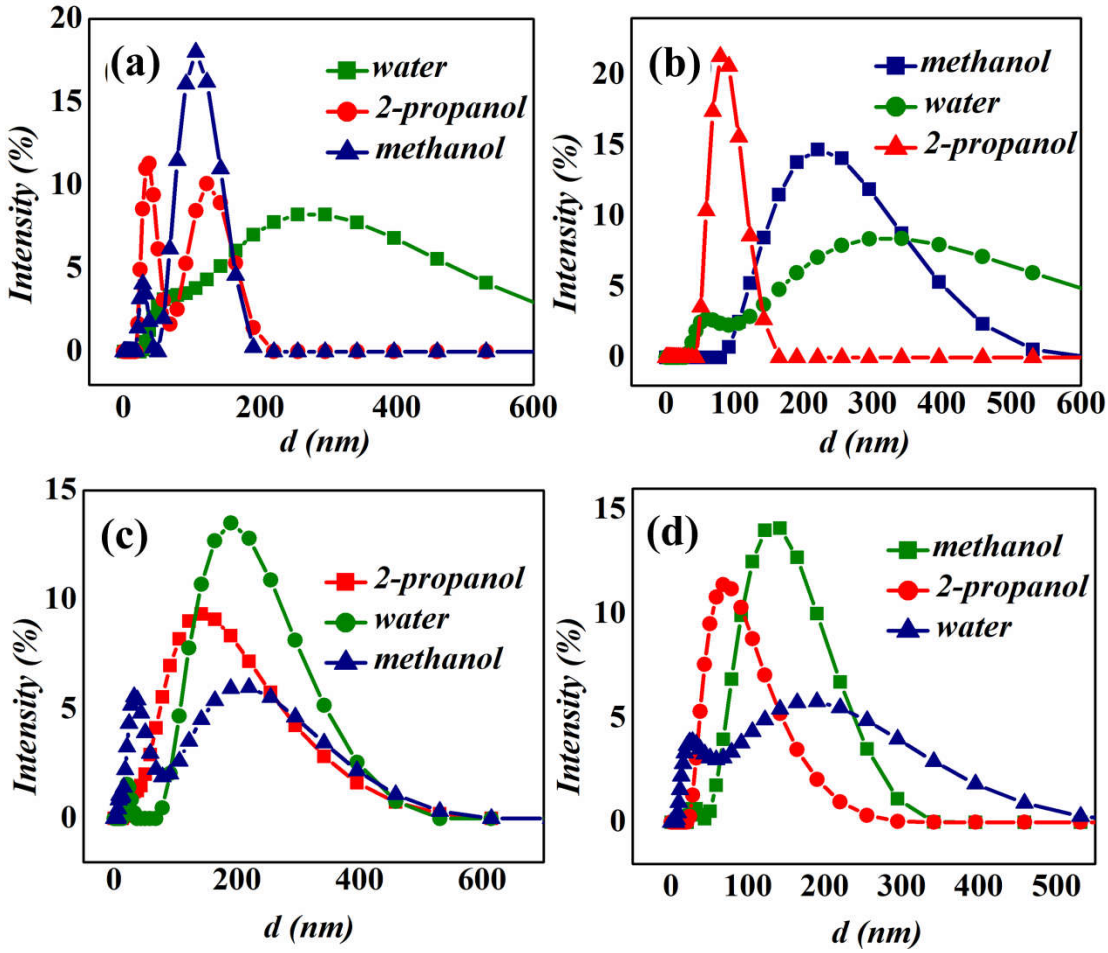

Figure 5.13. DLS profiles with average hydrodynamic radius of Pd/APTMS (a), Pd/EETMS (b), Au@PdNPs (c) and Ag@PdNPs (d) in water, methanol and 2-propanol.

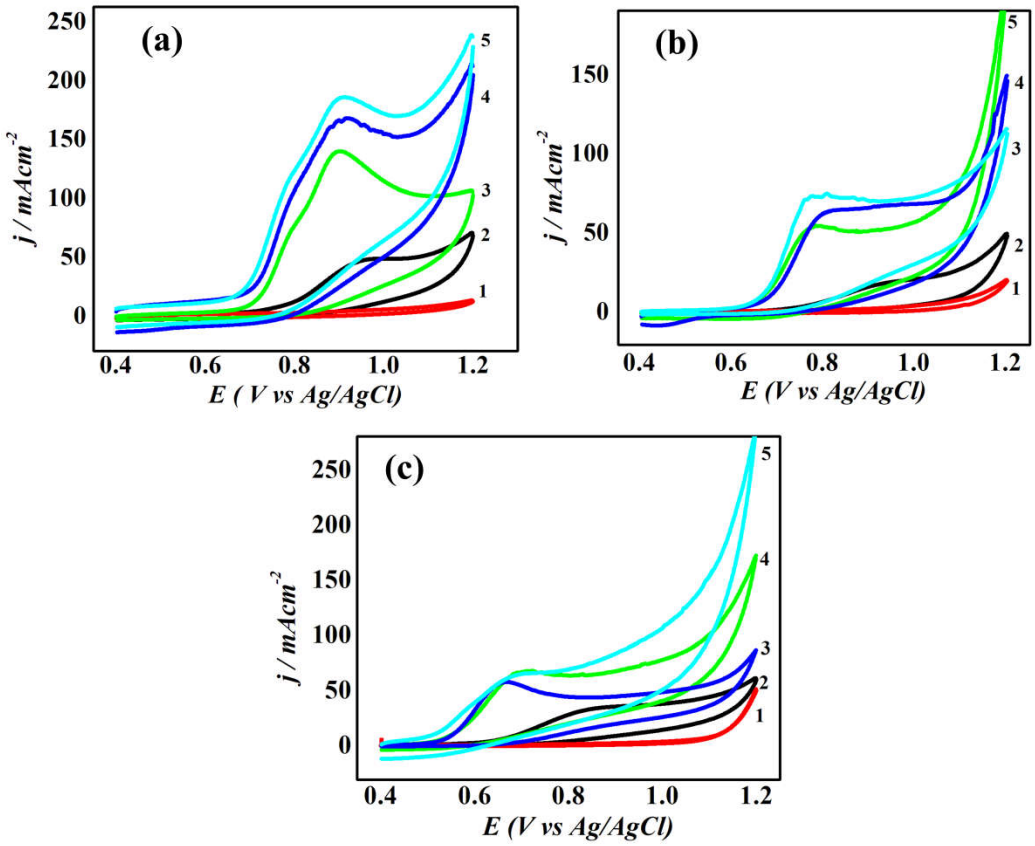

Figure 5.14. Cyclic voltammograms of 10 mM L-Trp in 0.1 M (a) pthallate buffer (pH-4.0), (b) phosphate buffer (pH-7.0), (c) borate buffer (pH-9.0), on (1) and (2) bare GCE with and without analyte, (3) Pd/GCE, (4) Au@Pd/GCE and (5) Ag@Pd/GCE, at a scan rate of 2 mVs^{-1}.

5.3.4. Differential pulse voltammetric measurements

In order to identify the possible mechanistic pathway of oxidation of L-Trp, a comparative study of nanocatalysts (PdNPs, Ag@PdNPs and Au@PdNPs) modified GCE in acidic, neutral and basic buffers was performed using differential pulse voltammetry (DPV). Peak current response at all investigated pH values (4, 7 and 9) were recorded, upon the addition of a wide range of concentrations (0.1 μM to 1000 μM) of L-Trp (Figure 5.16). DPV plots show the magnification in peak current with successive increase in analyte concentrations, at E = + 0.85, +0.78 and

+0.67 V, at pH 4, 7 and 9 over corresponding working electrodes (PdNPs, Au@PdNPs and AgNPs). The limit of detection for an effective range of analyte (L-Trp) concentration, 0.1 x 10^{-6} M to 1000 x 10^{-6} M at the Ag@PdNPs modified electrode was found to be 0.1 x 10^{-6} at pH-4, 0.5 x 10^{-6} at pH-7 and 9 respectively.

5.4. DISCUSSION

5.4.1. Functional alkoxysilane mediated synthesis of bifunctional nanoclusters

Stable Au@PdNPs and Ag@PdNPs are prepared by the combined action of alkoxysilanes, APTMS and EETMS. The role of these alkoxysilanes in the generation of nanoarrays on similar lines has been well documented in previous reports (Pandey et al, 2014; Pandey and Singh, 2015; Pandey and Pandey, 2016) of our lab. Here, the bimetallic nanoparticles of palladium are prepared by introducing the second metal (Au/Ag) in the crystal lattice of palladium. Ag and Au are chosen as the secondary metals because their lattice parameters [Au (0.408 nm) and Ag (0.409 nm)] coincide with that of Pd (0.38 nm). As evident from the TEM analysis, bimetallic nanocrystals (Au@Pd and Ag@PdNPs) have nearly core shell structure, where Au and Ag form the outer shell while palladium lies at the core. This stable arrangement of nanoscaled metal atoms attribute to the synergistic cooperation between the precursors, where APTMS and EETMS undergo specific interactions which was analyzed using FTIR spectroscopy (Figure 5.15). Bimetallic system posses a strong band at 1645.6 cm^{-1}, due to the formation of –C=C– linkage which was more prominent in 2-propanol, whereas the isolated mixture of alkoxysilanes exhibit a strong band at ~ 790-800 cm^{-1} (Si – O – Si) due to the rapid condensation and hydrolysis (Han et al., 2004).

These inferences justify that APTMS and EETMS behave differently in the presence of metal nanoparticles, specifically in 2-propanol to give monodispersed bimetallic nanocrystals, which further facilitated the development of uniform thin film over the substrates.

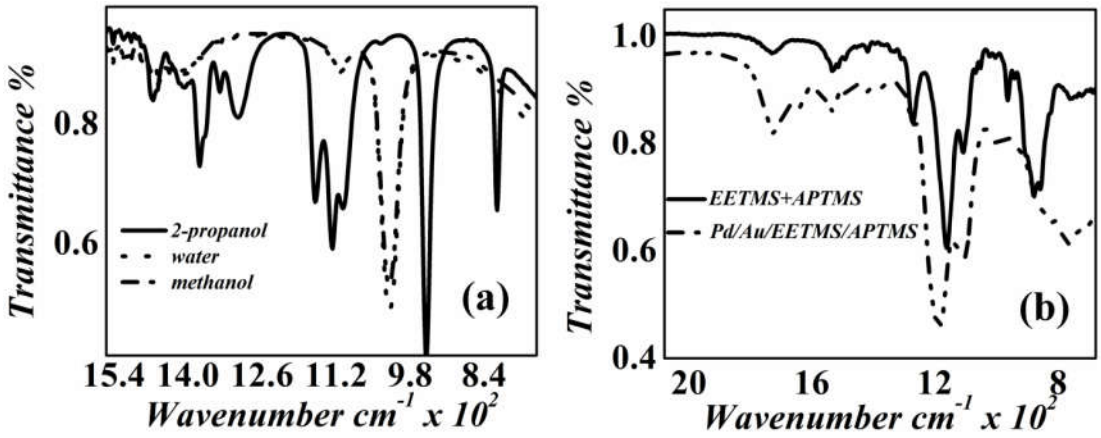

Figure 5.15. FTIR spectra of (a) bimetallic colloidal solutions in different solvents, (b) comparison of the interactions between EETMS and APTMS, in the presence and absence metallic species.

5.4.2. Synergistic action of solvents and Alkoxysilanes in thin film formation

The role of alkoxysilanes in deposition of uniform films of nanoparticles over the substrates was investigated in terms of variations in hydrodynamic radii (R_H), according to the solvent systems. The hydrodynamic radii of APTMS based PdNPs were found to be higher in contrast to that of EETMS based PdNPs, with lowest in 2-propanol, (water>methanol>2-propanol). This is due to the fact that EETMS being hydrophobic species with very high or negligible CMC values, does not undergo aggregation or micelle formation in alcoholic or aqueous media (Comas-Rojas et al, 2007). Similarly, PVP also has a large value of CMC, so self-aggregation is not detected. APTMS being amphiphilic in nature and having a finite value of CMC, often shows micellar behavior. Due to which there is a possibility of multiple layer formation in case of APTMS based PdNPs. The R_H values for BNPs were lower in alcoholic while higher in aqueous systems.

The trends obtained are a result of the variations in interaction forces in respective solvents. Hydrophobic organosilane (Pandey et al., 2005) systems involve three forces: electrical double layer (EDL), van der Waals forces, and hydrophobic forces (Hupka et al., 2010). In water-based system hydrophobic attraction forces are significantly long-range order (30 nm), which dominate over the repulsive ones. Therefore, the chances of the formation of electrical double layer are significantly high, and it is well supported by the hydrodynamic radius (R_H) (Table 5.1) and film thickness values (Table 5.2). While in alcoholic systems (2-propanol and methanol), both hydrophobic forces and EDL are weak, specifically in 2-propanol, only the hydrophobic repulsive forces are active (Hupka et al, 2010).

Table 5.1. Solvent dependent DLS profile of different nanoparticle systems.

Sample	**Solvents**					
	Water		**Methanol**		**2-Propanol**	
	R_H (d.nm)	**M_w/M_n**	**R_H (d.nm)**	**M_w/M_n**	**R_H (d.nm)**	**M_w/M_n**
Pd/EETMS	**263.2**	**0.29**	**180**	**0.24**	**86.68**	**0.166**
Pd/APTMS	**330.0**	**0.438**	**217.4**	**0.334**	**120.5**	**0.221**
Au@Pd/EETMS/ APTMS	**121.6**	**0.198**	**80.7**	**0.140**	**51.68**	**0.110**
Au@Pd/APTMS	-	-	-	-	**110.8**	**0.380**
Ag@Pd/EETMS/ APTMS	-	-	**82.6**	**0.144**	**66.5**	**0.154**

Thus, the chances of double layer formation are almost negligible in alcoholic systems. The sol-gel film constitutes an array of heterogenous structures, arranged in nanoporous domains aligned in a perpendicular fashion to the substrate surface as evident from the AFM topographical spectra (Figure 5.10-5.12). Micellar films of bimetallic systems synthesized in water and methanol are short-range order rather than the propanol based systems, due to relatively high polydispersity of objects in water and methanol. Irregular structures are obtained on the deposition of water-based bulk solutions, which involves polydispersed objects, while the controlled filling of the substrate surface is seen in other systems (Figure 5.10-5.12). The degree of uniform spread of the colloidal solution depends on the threshold of formation of objects in solution.

Dependency on solvent is indirectly related to certain variables, like interaction forces, critical surface tension, adhesion property, wettability and contact angle, which are in turn ultimately pivoted to the material of the thin film formation. Since we explore the role of alkoxysilanes in the development of functional nanostructured lattices of self assembled bifunctional nanomaterials, literature reports that organofunctionalised alkoxysilanes have a tendency to form silanol containing species on hydrolysis. In aqueous media hydrophobic forces and hydrogen bonding are dominant interactions between EETMS and APTMS, and they promote the adhesion, with the possibility of multilayer deposition. Higher content of water is the driving force for accelerating the rate of condensation, which subsequently facilitates the generation of oligomeric or polymeric Si – O – Si linked chains, resulting into deposition of multilayers (Bunker et al., 2000). Therefore, for preferential monolayer deposition, rate of condensation need to be controlled, which is done possibly by maintaining anhydrous conditions at the solution-

substrate interface as well as in bulk solutions. While in alcoholic solutions with reduced water content only hydrophobic forces are dominant short range attractive forces. Thus in order to achieve the required nanostructured lattices, we have synthesized the film forming bulk solutions using alcoholic solvents (methanol, propanol) and compared with those of water-based systems. The water content in the alcoholic systems has been remarkably reduced to about 10^{-6} M, therefore these materials build their capacity to wet the hydrophobic surfaces with ease.

Table 5.2. Comparision of solvent dependent properties of thin films.

Sample Thin Film	Solvents	Film thickness (nm)	Pore density (%)	RMS Rsq (nm)
Pd/EETMS	Water	14	15	0.445
	Methanol	11	20	0.189
	2-Propanol	8	26	0.134
Au@Pd/EETMS/	Water	13.5	20	0.225
APTMS	Methanol	10.6	32	0.184
	2-Propanol	7	40	0.122
Ag@Pd/EETMS/	Water	12	18	0.221
APTMS	Methanol	10	27	0.162
	2-Propanol	6	35	0.129

Although the silane-based nanostructured thin films turns the substrate surfaces hydrophobic (high contact angles 49-100º) (Han et al., 2004; Jin et al., 2011), but it is reported that the contact angle parameter is not the principle indicator of the wettability by liquids other than water, such as salt or buffer solutions, which have high surface tensions (Jin et al, 2011). In fact, surfaces modified with alkoxysilanes (EETMS, APTMS) have high lower critical surface tensions (28-42 dynes/cm), and in studies carried out by various researchers in recent decades prove that the surfaces with low surface tension are active in high surface tension solutions and solvents. Therefore, the propanol based core structured bimetallic nanoparticles (Au@PdNPs, Ag@PdNPs) generated due to interactions between PVP, EETMS and micellar behavior of APTMS, facilitate the fabrication of regular and ordered pattern of close-packed structures are formed in the solution and preferential nanoporous self-configured sol-gel thin films.

5.4.3. Electrochemical oxidation of L-Tryptophan

The nanoporous thin films are allowed to grow on the surface of glassy carbon electrode (GCE) and tried as working electrodes for evaluating the oxidation behavior (MacDonald and Roscoe, 1997; Fiorucci and Cavalheiro, 2002; Wang and Chen; 2003; Enache and Oliveira-Brett, 2011) of L-Trp. The thin film modified electrodes facilitate the oxidation of amino acid to occur at thermodynamically favoured and lower potentials with considerable amplification in current density (Figure 5.14a-c). It is reported that the L-Trp undergoes pH dependent electroxidation, so it is observed in the present study, at pH > 4, the oxidation peak of L-Trp is shifted to lower potentials while at lower pH the oxidation occurs at higher potentials. This occurs due to the complex metabolism of L-Trp at different pH.

5.4.4. DPV analysis

Figures 5.16-5.18 represents the typical DPV plots and the corresponding current densities versus relative concentration plots (calibration curves). Peak current fortunately increased as a function of concentration of analyte, with successive DPVs recorded for constant time intervals. The oxidation of L-Trp using noble metal nanocatalysts modified electrode gives only one oxidation peak. Maximum peak current density was observed in case of Ag@PdNPs modified electrode.

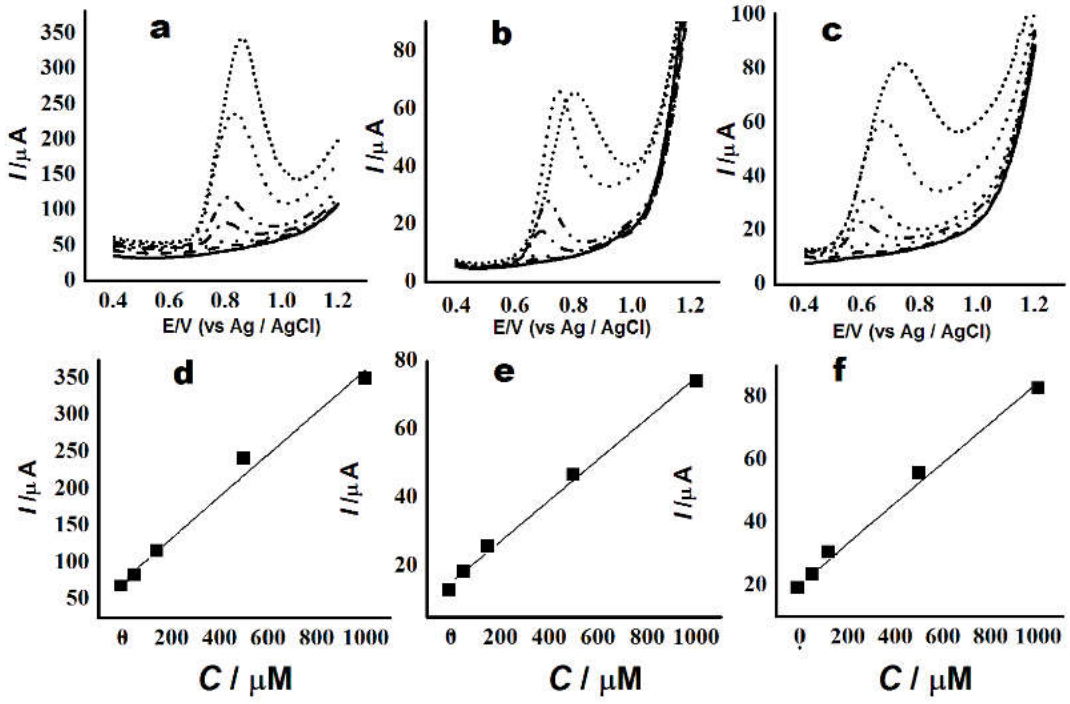

Figure 5.16. DPV curves of L-Trp on Pd/GCE at (a) pH 4, (b) pH 7 and (c) pH 9, with concentrations ranging from 0.1μM to 1000 μM. (d)-(f) Corresponding calibration curves of L-Trp.

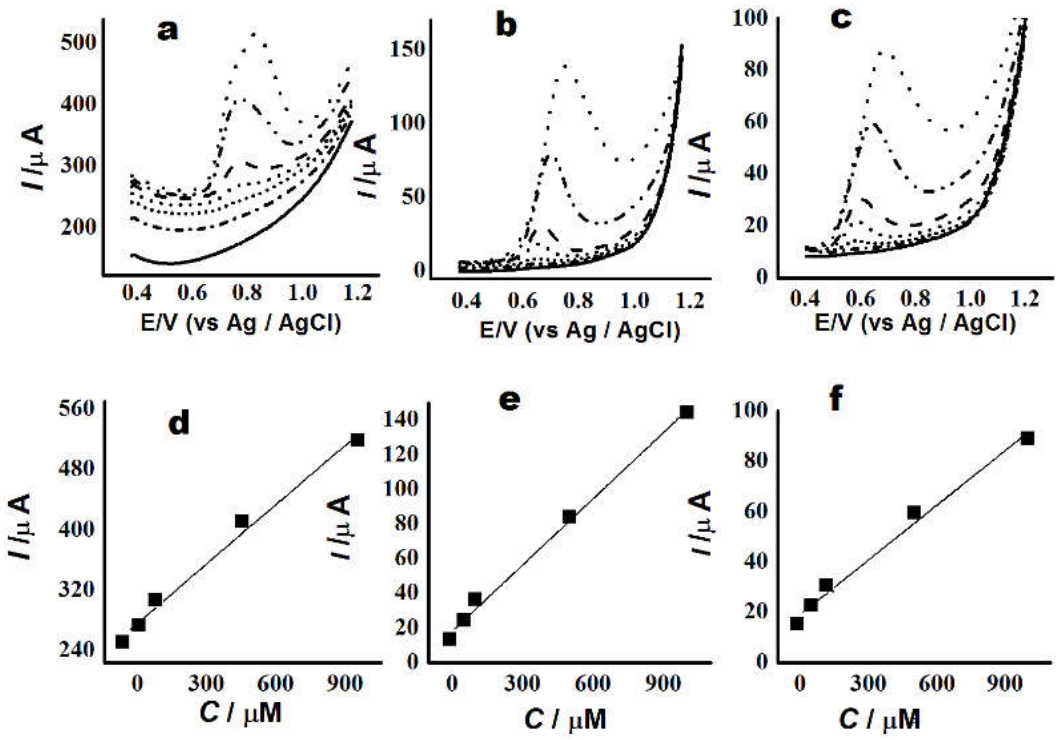

Figure 5.17. DPV curves of L-Trp on Au@PdNPs/GCE at (a) pH 4, (b) pH 7 and (c) pH 9, with concentrations ranging from 0.1μM to 1000 μM. (d)-(f) Corresponding calibration curves of L-Trp.

The single peak for electroxidation of L-Trp at different pH, and the values of $W_{1/2}$ lying between ~ 90-100 mV, correspond to that of single electron transfer reaction (Wang and Chen; 2003; Enache and Oliveira-Brett, 2011). The high detection limits (LOD) were recorded for Au@PdNPs modified electrodes, as 5 x 10^{-6}, 10 x 10^{-6} and 10 x 10^{-6} at pH-4, 7 and 9 and even higher values, 10 x 10^{-6}, 50 x 10^{-6}, and 50 x 10^{-6}, at pH-4, 7 and 9, are observed for PdNPs modified electrodes, on subjecting to equivalent concentration spectrum of analyte, while the lowest detection limits were observed in case of Ag@PdNP are as 1 x 10^{-6}, 1 x 10^{-6} and 5 x 10^{-6} at pH-4, 7 and 9.

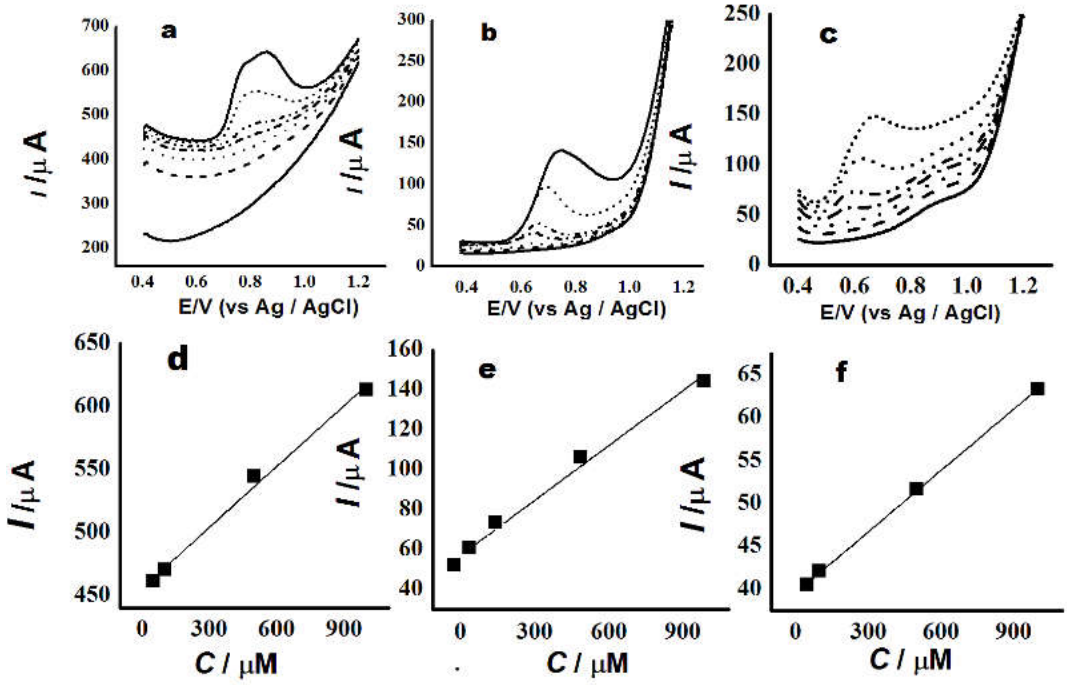

Figure 5.18. DPV curves of L-Trp on Ag@PdNPs/GCE at (a) pH 4, (b) pH 7 and (c) pH 9, with concentrations ranging from 0.1μM to 1000 μM. (d)-(f) Corresponding calibration curves of L-Trp.

5.5. CONCLUSION

This chapter demonstrates a flexible approach to synthesize binary nanoscaled materials and self-assemble the bifunctional materials on solid substrates by means of well-defined orientation of organofunctionalised alkoxysilanes into nanostructured thin films, via a multistep guided process. Initially, EETMS stabilized PdNPs are synthesized in water, methanol, and 2-propanol, further, hybrid bifunctional nanomaterials (Au@PdNPs, Ag@PdNPs) are prepared through sequential synthesis using PdNPs as a template, which are stabilized by the micellar behavior of APTMS. EETMS/APTMS based Au@PdNPs in propanol has the lowest hydrodynamic radii and polydispersity index. The hydrodynamic radius of the objects formed; vary according to the interactions between alkoxysilanes and solvents. Hence, we manifest a route to manipulate the

surface topography of the film, thereby controlling the composition of alkoxysilanes (EETMS, APTMS) and solvent selection. Thus, the self-configured assembly of bifunctional materials into a patterned array, with precisely controlled nanogeometry of the constituent particles is considered to be the possible arrangement for potential catalytic applications.